Energy, Volume 185, Issue October, 2019, pp. 730-743
DOI: 10.1016/j.energy.2019.07.054

Modelling and simulation of steel reheating processes under oxy-fuel combustion conditions – Technical and environmental perspectives

Yukun Hu[a*], CK Tan[b], John Niska[c], Jahedul Islam Chowdhury[a,d], Nazmiye Balta-Ozkan[d], Liz Varga[a], Paul Alun Roach[b], Chunsheng Wang[e]

[a] Department of Civil, Environmental & Geomatic Engineering, University College London, London WC1E 6BT, UK

[b] Faculty of Computing, Engineering and Science, University of South Wales, Pontypridd CF37 1DL, UK

[c] Swerim AB, Box 812, Luleå SE-25, Sweden

[d] School of Water, Energy and Eviornment, Cranfield University, Bedford MK43 0AL, UK

[e] School of Information Science and Engineering, Central South University, Changsha, 410083, China

Abstract

This paper investigates the impact of flameless oxy-fuel combustion on the thermal performance of a pilot-scale steel reheating furnace. A comprehensive mathematical model, based on the zone method of radiation analysis, was developed, which takes into account the non-grey behaviour of the furnace atmosphere under oxy-fuel combustion conditions. The model was subsequently used to simulate the temperature profile of an instrumented slab used in the experiment. The results showed that the predicted slab temperature profile along the furnace is in good agreement with measurement. However the model over predicted the absolute slab temperatures due to the influence of formation of oxide scales on the slab surface, which was not taken into account in the current model. When compared to air-fuel combustion simulation, the results of oxy-fuel combustion also indicated a marked improvement in the furnace specific fuel consumption (approximately 16%). This was mainly due to the enhanced radiative properties of the furnace atmosphere and reduced exhaust energy losses as the result of less dilution effect from nitrogen. This resulted in reduction in the overall heating time by approximately 14 minutes. Furthermore, if the economics of carbon capture is taken into consideration, theoretically, the energy consumption per kilogram of CO_2 captured can be reduced from 3.5–4.2 MJ kg^{-1} to 0.96 MJ kg^{-1}. In conclusion, the current studies support the view that oxy-fuel combustion retrofitting to reheating furnaces is a promising option, both from a technical and from an environmental point of view.

Keywords: reheating furnace; air-fuel combustion; flameless oxy-fuel combustion; zone method; thermal performance

* Corresponding author. E-mail address: yukun.hu@ucl.ac.uk, ceykhu@gmail.com (Y. Hu)

Published by Elsevier. This is the Author Accepted Manuscript issued with: Creative Commons Attribution Non-Commercial No Derivatives License (CC:BY:NC:ND 4.0). The final published version (version of record) is available online at DOI:10.1016/j.energy.2019.07.054. Please refer to any applicable publisher terms of use.

1. Introduction

Rising concerns about energy demand and CO_2 emissions are prompting increased efforts to achieve sustainable development in energy intensive industries. The iron and steel industry is one of the largest energy consumers in the industrial sector, accounting for about 18% of delivered industrial sector energy use from non-OECD countries in 2012, and predicted to still account for about 14% in 2040 (Figure 1). Although modern integrated iron and steel-making plants tend to be more energy efficient, the International Energy Agency reported in 2012 [1] that there is still the potential for the iron and steel industry to reduce its current total energy consumption by approximately 20% through applying the best available technologies in energy efficiency and waste heat recovery [2]. In a typical integrated steel plant, the energy consumption is distributed into roughly 70% for iron and steel production, 20% for rolling, and 10% for miscellaneous consumption such as lighting and air conditioning [3]. In particular, reheating furnaces are used extensively to heat intermediate steel products such as slabs, billets or blooms (known as stock) to a specified temperature and through-thickness temperature uniformity prior to hot-rolling. Energy consumption in reheating furnaces depends on many operating factors, such as production scheduling [4,5], furnace set-point temperatures [6,7], control algorithms [8,9], and waste heat recovery [10,11]. Therefore, much effort has been made around these aspects to improve their energy efficiency [12] and carbon mitigation [13]. However, today's best practice values for heating a tonne of steel to the right temperature for rolling or forging is still above 1.0 GJ/tonne [14]. If no substantial upgrading of existing combustion technologies is put in place, furnace operators will likely struggle to achieve further reduction in fuel consumption and CO_2 emission [15]. This is due to the inherent negative impact of nitrogen (which is the main constituent of air) on the combustion process that could lead to a decrease in heat transfer efficiency and excessive heat loss through the exhaust gas. Consequently, oxy-fuel combustion has been considered by many to be an attractive alternative combustion technology to alleviate the above bottleneck.

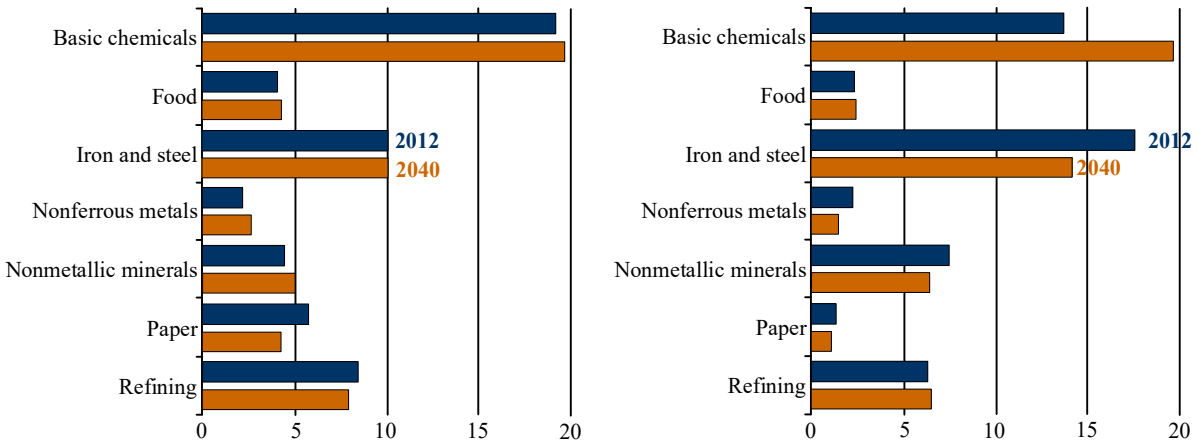

Figure 1. Energy-intensive industry shares of total OECD (left) and non-OECD (right) industrial sector energy consumption, 2012 and 2040 (percent of total) [16]

For more than 150 years, the benefits of using oxygen in steel-making have been recognised, since Sir Henry Bessemer referred to the possibilities of oxygen in his patent for the Bessemer process [17]. The benefits include better transfer and utilisation of heat, higher reaction temperature and an

increased rate of oxidising reactions [18]. However, it was not until the early 1900s when Carl von Linde patented his large-scale oxygen production technology [19] that the way was paved for the subsequent development of the basic oxygen steelmaking process [20]. Over the past 50 years, the cost of oxygen production has decreased by 50% while production capacity has been more than quadrupled to 4,500 tons per day, as shown in Figure 2. With oxygen becoming more affordable, Abraham [21] proposed the concept of oxy-fuel combustion to produce a CO_2 rich flue gas in the context of effective carbon-capture from large emission sources [22]. More recently, oxy-fuel combustion technology has also received much attention in steel-making plants, particularly for reheating and annealing processes.

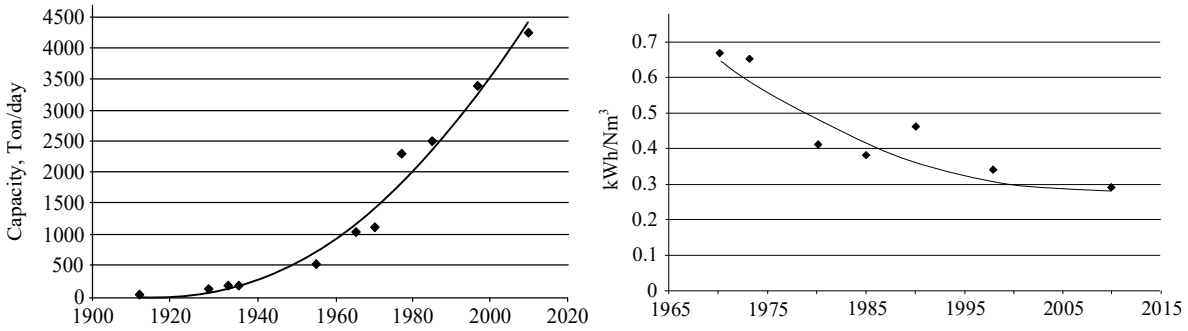

(a) (b)

Figure 2. History of oxygen production capacity (a) and cost (b) (adapted from [23])

One of the earliest studies of oxy-fuel combustion applied to reheating furnaces is the US Department of Energy (DoE) 'Dilute oxygen combustion (DOC)' project conducted by Praxair Inc. in the 1990-2000s. The novel DOC burner developed was characterized by separate injection of fuel and oxidant into the furnace [24], a process having similarities to flue gas recirculation (FGR) techniques [15] but with dilution being achieved using the entrainment characteristics of turbulent jets. Although a furnace fired completely with DOC burners offers low capital cost, low fuel rate, and minimal NOx emissions [25], these benefits did not offset the cost of oxygen at that time ($23 per tonne); a full DOC-fired furnace was projected to cost $1.30 per ton more to operate than a conventional air-fired furnace [26]. Therefore, technical efforts have concentrated on passive means of improving thermal efficiency of DOC burners, such as self-recuperative burners and regenerative combustion [27]. For example, an efficient heat recovery method using rapid cycle regenerators for oxy-fuel fired DOC burners was proposed [28], in which a mixture of natural gas and recycled flue gas undergoes endothermic carbon dioxide and steam reforming reactions in the regenerator. To date, Praxair DOC systems have been successfully installed on various industrial furnaces including continuous steel reheating furnaces and batch reheating furnaces. Nowadays, other variants of DOC technology, more commonly known as flameless oxy-fuel combustion, have been successfully applied in various high-temperature furnaces [29–32] where high heat transfer efficiency and temperature uniformity, and low NOx emissions are crucial. In particular, in steel reheating applications, the highly uniform heat distribution pattern within furnace also contributes to overall reduction in the heating time and hence specific fuel consumption [33–35]. To maximise the above perceived benefits, an adequate understanding is required of the behaviour of oxy-fuel combustion, particularly its influence on the radiative characteristics of the furnace atmosphere, as well as its interaction with the furnace space and set-point temperature control [36].

With regard to furnace temperature control, the set-point temperatures in various heating zones are regulated by comparing the desired and predicted heating curves. However, the desired heating curve depends on designed operating conditions under steady-state and is rarely published [9]. Furthermore, there are still technical challenges posed by oxy-fuel combustion retrofitting in reheating furnaces in practice, especially in how to optimise the furnace set-point thermocouple locations and/or set-point temperatures to avoid under- or over-heating the discharged product. So far, there are only a few comprehensive works reported in the literature related to modelling and simulation of heat transfer in reheating furnaces under oxy-fuel combustion conditions. Oliveira et al. [15] explore the possibilities of oxy-fuel combustion as an alternative to combustion with air in metal reheating furnaces from a techno-economic point of view. Prieler et al. [37] numerically analyse the reheating process under air-fired and oxygen enriched conditions by coupling steady state gas combustion in the furnace and the transient heat conduction within the steel billets. Han et al. [38] analyse the efficiency of air-fuel and oxy-fuel combustion in a reheating furnace, considering only thermal radiation for the slab heating. However, none of these studies consider full transient simulations of the whole furnace and interaction with responses of the temperature control system.

To better explore the impact of flameless oxy-fuel combustion technology, two experiments were conducted on a pilot-scale reheating furnace under both air-fuel and oxy-fuel combustion environments at Swerim (former Swerea MEFOS), Sweden. Measurement data gathered from these experiments were used to validate a comprehensive mathematical model, which takes into account detailed physics of the heat transfer processes within the reheating furnace. A particular novelty of the current work is the appropriate treatment of the non-grey behaviour of radiating gases under oxy-fuel combustion atmosphere. The developed model may be used for offline (but still relatively fast) tools by furnace operators to investigate more generic aspects of furnace operation and control. The paper is structured as follows: Section 2 reviews previous work on reheating furnace modelling, process control, and operation optimisation. Section 3 outlines the scope for simulation of the pilot trials, including furnace geometry and operations. Section 4 presents the furnace model development and the estimation of mixed gas emissivity under different combustion environments. Section 5 presents the results and analysis of the simulated furnace operation described in Section 3. Section 6 discusses the potential benefits of oxy-fuel combustion retrofitting in reheating furnaces from a carbon capture point of view. Finally, in Section 7, conclusions in relation to this overall study are drawn, along with recommendations for future work.

2. Previous work on zone modelling of reheating furnaces

Mathematical models that are capable of predicting thermal performances of high-temperature furnaces from the fundamental laws of physics have been available for many years. Most furnace models are based on either computational fluid dynamic (CFD), so-called CFD models [39,40], or zone method of radiation analysis [41], so-called zone models. The prediction of fluid flow using CFD involves the simultaneous solution of the Navier-stokes equations for momentum conservation together with the equations for mass conservation in each of the relevant co-ordinate directions. If turbulent combusting flows are to be simulated, conservation equations for enthalpy and chemical species should also be added. However, CFD models are relatively inefficient, especially when full furnace transient simulations are necessary to take into account responses of the furnace temperature

control system. In contrast, zone models can provide an accurate representation of non-grey radiation exchange within furnace enclosure, even with relatively fewer cells than that would be required by the CFD model. However, the zone model does not calculate fluid flow, mixing and chemical kinetics governing the combustion of fuel, which must be supplied from other sources. The main advantage of the zone model lies in its simplicity and efficiency, when detailed furnace flow pattern is not mandatory to achieve acceptable accuracy of prediction of the thermal performance of furnaces. The following sub-sections serve to provide a brief overview of the recent development and application of zone modelling in reheating furnaces, paying particular attention to integration of furnace flow data, radiation exchange areas calculation, process control and optimisation.

2.1 Flow data generation

When Hottel and Sarofim [41] first proposed the zone method for radiation analysis, they assumed five different flow patterns in a cylindrical end-fired furnace: plug flow; a parabolic self-perpetuating velocity profile; and three ducted-jet flow patterns. Through incorporating these flow patterns, the zone model was able to predict radiation heat transfer of almost any degree of complexity involved in this simple geometry. Many of the early applications of the zone model were documented in a monograph jointly published by Rhine and Tucker [42]. While both one and two-dimensional zone models can be easily applied with relatively simple furnace flow patterns, for more complex flow patterns, which are normally required in practice, a three-dimensional zone model is necessary. In such cases, the three-dimensional flow data may be obtained from solutions of steady-state isothermal CFD simulation. In order to allow for full transient simulation, in which the furnace flow pattern may vary from one instance to another, Hu et al. [8] have pioneered the use of Box–Behnken response-surface approach to develop a fast quadratic flow model. The model data were obtained from a series of steady-state isothermal CFD simulations that span the whole range of the furnace operating conditions [43]. The resultant flow model was thus able to interpolate between steady-state flow fields (albeit approximately) during a typical time interval of a transient furnace simulation.

2.2 Radiation exchange area calculation

The concept of radiation view factor forms the basis for calculating the various radiation exchange areas required by the zone model, such as direct exchange areas, total exchange areas, and directed flux areas [42]. For complex furnace geometry, Monte Carlo ray-tracing [44] is a preferred method for calculating radiation view factor. This is accomplished by tracing the paths followed by a large number of randomly distributed and diffused bundle of rays from a surface or volume zone, until they are ultimately intercepted by all other possible surface and volume zones within the furnace enclosure. Due to the statistically approximate nature of the Monte Carlo method, it is necessary to ‘smooth’ the results to ensure compliance with the summation and reciprocity rules [45]. Lawson [46] developed a flexible computer program, called RADEX, which allows users to quickly set up geometries and output arrays of exchange areas which can be readily imported into any third-party programming software. However, the output from RADEX has no facility for tracking movement of individual stock pieces in the context of a continuously operated reheating furnace. Consequently, Matthew et al. [47] developed a more flexible version called REFORM, which had removed such restrictions in RADEX. Hu et al. [8] further improved the computational efficiency of the REFORM program using parallel computing algorithms [48], employing this in their more recent work [49].

2.3 Process control algorithm

Much of the early work with regard to simulation of furnace control was based on idealised two-position or proportional temperature control algorithms [42], which can be easily incorporated into the logic of a furnace model by relating the fuel input rate to the deviation from a set-point temperature. However, due to the characteristics of the proportional controller, it cannot eliminate the offset error, i.e. the difference between the desired value and the actual value, as it requires an error to generate an output. To overcome this disadvantage, Hu et al. [8] developed a normalised proportional–integral–derivative (PID) control algorithm. In this algorithm, the required temperature compensation relative to the set-point temperature at the current time-step is used to adjust the burner fuel flow rate in the beginning of the next time-step through a normaliser (i.e. normalising the firing rate between 0 and 1). This control algorithm was incorporated into a zone model to simulate a period of real furnace operation. The result showed that predictions from the developed control model outperformed those of the existing level-2 model in most instances. Based on this work, Hu et al. [9] further developed a combined feedforward and feedback set-point temperature control algorithm to adjust the furnace set-point temperatures in response to changes in operation, in which non-uniform batch scheduling and production delay were encountered.

2.4 Optimisation of heating profile

Traditionally, linear empirical models have been used to optimise the furnace control scheme, i.e., by minimising the deviation between the desired and actual (albeit predicted) stock temperature profile. They usually involve gathering a representative amount of actual plant data from which, through the use of appropriate system identification tools such as deterministic regression [50] or artificial intelligent techniques [51–53], an approximate model of the actual process is derived. However, these types of model, although superior in computational speed, suffer from a limited scope of operating conditions beyond which the risk of misrepresentation to the actual process behaviour may be too significant. This is because the actual physics of the heating processes is not inherently encapsulated within their associated mathematical formulation. To address this limitation, Hu et al. [6] proposed a zone model based multi-objective optimisation of reheating furnace operations, and highlighted a novel approach of incorporating the zone model directly into a population based genetic algorithm to optimise the desired stock heating curve for a given set of process constraints relating to energy consumption and/or product quality. The results showed that the proposed optimisation strategies can improve heating accuracy (the average deviation was less than 10 °C from the desired discharge temperature), while a trade-off was shown to exist between the optimization objectives of temperature uniformity and specific fuel consumption.

3. Scope for simulation of the pilot trials

The experiments were conducted on a pilot-scale walking beam top-fired furnace (Figure 3), with a production capacity of 3 tonne/hr and a target heating temperature of 1250 °C. The furnace dimension is 9 m long and 2.2 m wide, while the furnace height varies across different furnace zones, rising up to 1.8 m above the walking beams in heating zone as shown in Figure 4. The furnace is divided into an unfired preheating zone (dark zone), three heating zones (or control zones) and a soaking zone. Each of the three control zones (CZs) is equipped with pairs of burners on opposite sides. The furnace is extensively instrumented to allow for detailed monitoring and control of the steel reheating process. Specifically, the furnace crown temperature profile was monitored by roof thermocouples (Type S/R,

standard accuracy: ±1.5C or ±0.25%), which were used for controlling the power input to the furnace. A dummy slab was instrumented with five thermocouples (Type N, standard accuracy: ±2.2C or ±0.75%) to monitor the temperature distribution inside the slab during its passage through the furnace, see Figure 3. It should be noted that during the oxy-fuel combustion experiment the reliability of thermocouple-TC2 was compromised towards the end, possibly due to over-heating. As a result, thermocouple-TC4 was used instead for comparison with the predicted temperature at the centre of the slab. The furnace was initially filled with a total of 17 slabs (0.155m×0.4m×1.7m, 7800 kg/m^3) and heated until the normal operating temperature of the furnace was attained. The dummy slab, along with others, were subsequently charged into the furnace until the end of each test to simulate a continuous reheating operation. A flow control rack which used Yokogawa digital Yewflo vortex flow meters [54] (standard accuracy: ±1%) was used for gas flow measurements in the trial. The specific operating conditions used in both oxy-fuel and air-fuel combustion modelling are listed in Table 1.

Figure 3. Images of the pilot-scale walking beam furnace (top) and the instrumented slabs with thermocouples (bottom)

Table 1. Operation conditions of two different trials

	Energy input		Set-point temperatures			Excess oxidant	Partial pressure	Stoich. ratio
	Type of Fuel, -	LHV, MJ/kg	CZ1, °C	CZ2, °C	CZ3, °C	-	(P_{H2O}+P_{CO2}), atm	(air/fuel), -
Air-fuel	Light fuel oil	42.9	955	1220	1250	10.0 (air)	0.248	14.4
Oxy-fuel	Propane	46.4	1040	1220	1250	4.0 (oxy)	0.971	N/A

4. Model development

Based on previous experience in modelling air-fuel operation, the furnace enclosure was divided into 12 sections (across its length) × 2 sections (across its height) × 1 sections (across its width), which was found to be adequate[1]. In total there are 24 volume zones and 178 surface zones (including 76 surface zones for furnace walls and 102 surface zones for slab surfaces), as shown in Figure 4. The momentum supplied by the burners ensures a high rate of mixing and the flame occupies a small fraction of the zone volume, hence it is reasonable to assume that the gas is perfectly well-stirred in each volume zone. In this case, the mean radiating beam length [55] can be based on the zone volume and its bounding surfaces, and the radiation characteristics from a surface zone (furnace wall or slab surface) can therefore be completely specified by the mean beam length, the surface areas, and the partial pressures of all radiating gases. Then, an energy balance can be formulated for each volume and surface zone taking into account radiation interchange between all zones, the enthalpy transport, source terms associated with the flow of combustion products and their heat release due to combustion [42].

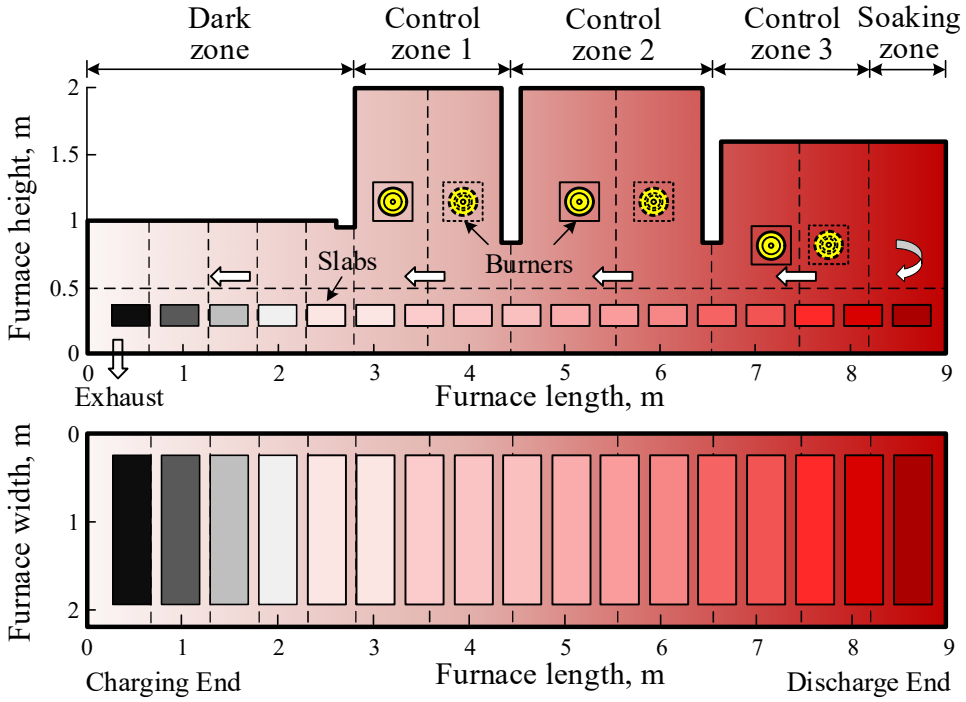

Figure 4. Outline of the furnace and zoning arrangement (in scale)

[1] The principle of zoning is to make the volume and/or area of each zone as comparable as possible and for each burner to be contained in a single zone.

For a model comprising M surface zones and N volume zones, the energy balance (in energy unit of *Watt*) on the i-th surface zone, which may be an internal wall or a slab surface and which has area denoted A_i, can be written as *Eq*. 1:

$$\sum_{\mathrm{j}=1}^{M} \overleftarrow{S_\mathrm{i}S_\mathrm{j}}\sigma T_{\mathrm{s,j}}^4 + \sum_{\mathrm{j}=1}^{N} \overleftarrow{S_\mathrm{i}G_\mathrm{j}}\,\sigma T_{\mathrm{g,j}}^4 - A_\mathrm{i}\varepsilon_\mathrm{i}\sigma T_{\mathrm{s,i}}^4 + A_\mathrm{i}(\dot{q}_{\mathrm{conv}})_\mathrm{i} = \dot{Q}_{\mathrm{s,i}}. \qquad (Eq.\ 1)$$

The first term in *Eq*. 1 is the sum of the arriving radiation from all surface zones (including zone i). The second term is the sum of the radiation from all volume zones. The third term is the total radiation leaving surface zone i. The fourth term is the convective heat transfer to surface zone i. Therefore, the last term equals the net rate of heat transfer to surface zone i. Finally, $\dot{Q}_{\mathrm{s,i}}$ can be expressed in term of temperature of surface zone i via solution of transient conduction through the associated furnace wall or slab section.

Likewise, energy balance equations (*Eq*. 2) can also be written for the volume zones.

$$\sum_{\mathrm{j}=1}^{N} \overleftarrow{G_\mathrm{i}G_\mathrm{j}}\sigma T_{\mathrm{g,j}}^4 + \sum_{\mathrm{j}=1}^{M} \overleftarrow{G_\mathrm{i}S_\mathrm{j}}\,\sigma T_{\mathrm{s,j}}^4 - 4\sum_{\mathrm{n}=1}^{n_\mathrm{g}} a_{\mathrm{g,n}}\,k_{\mathrm{g,n}}V_\mathrm{i}\sigma T_{\mathrm{g,i}}^4 - \left(\dot{Q}_{\mathrm{conv}}\right)_\mathrm{i} + (\dot{Q}_{\mathrm{fuel,net}})_\mathrm{i} \qquad (Eq.\ 2)$$
$$+(\dot{Q}_\mathrm{a})_\mathrm{i} + (\dot{Q}_{\mathrm{enth}})_\mathrm{i} = 0.$$

The first two terms in *Eq*. 2 are the sum of the arriving radiation from all gas (volume) zones and surface zones respectively. The third is the total radiation leaving gas zone i. $\dot{Q}_{\mathrm{conv}}$ is the convection heat transfer to all bounded surfaces of gas zone i. $\dot{Q}_{\mathrm{fuel,net}}$ is the heat release due to combustion within gas zone i. $\dot{Q}_\mathrm{a}$ is the thermal input from the preheated combustion air (or oxygen in the case of oxy-fuel combustion). $\dot{Q}_{\mathrm{enth,net}}$ is the net enthalpy exchange in gas zone i due to mass transfer.

The above equations are written in terms of directed flux areas (denoted by $\overleftarrow{G_\imath G_J}$, $\overleftarrow{S_\imath G_J}$, $\overleftarrow{S_\imath S_J}$ and $\overleftarrow{G_\imath S_J}$). These directed flux areas, which allow for the effects of surface emissivity and the non-grey behaviour of the radiant interchange within the furnace enclosure, are defined as follows:

$$\overleftarrow{G_\imath G_J} = \sum_{n=1}^{N_g} a_{g,n}\left(T_{g,j}\right)\left(\overline{G_\imath G_J}\right)_{K=K_n} \qquad (Eq.\ 3)$$

$$\overleftarrow{S_\imath G_J} = \sum_{n=1}^{N_g} a_{g,n}\left(T_{g,j}\right)\left(\overline{S_\imath G_J}\right)_{K=K_n} \qquad (Eq.\ 4)$$

$$\overleftarrow{S_\imath S_J} = \sum_{n=1}^{N_g} a_{s,n}\left(T_{s,j}\right)\left(\overline{S_\imath S_J}\right)_{K=K_n} \qquad (Eq.\ 5)$$

$$\overleftarrow{G_\imath S_J} = \sum_{n=1}^{N_g} a_{s,n}\left(T_{s,j}\right)\left(\overline{G_\imath S_J}\right)_{K=K_n} \qquad (Eq.\ 6)$$

where $\overline{G_i G_j}$, $\overline{S_i S_j}$ and $\overline{G_i S_j}\ (=\overline{S_i G_j})$ are the total exchange areas and. $a_{g,n}$ and $a_{s,n}$ are the weighting coefficients which can be interpreted as the fraction of the radiant energy associated with each of the n-th grey gases. These weighting coefficients are generally expressed as a low-order polynomial in T_g and T_s, as discussed in more detail subsequently.

The energy balances on all zones yield $M + N$ non-linear simultaneous equations in $M + N$ unknown surface and gas zone temperatures, which can be solved efficiently by applying Newton Raphson method [56]. The solutions of these temperatures then enable calculations of the heat flux on each surface zone. The calculated surface heat fluxes then serve as boundary conditions for solution of transient heat conduction through the furnace walls and slabs [8]. The nodal temperatures for all the wall and slab sections are then updated accordingly at every iteration of the transient simulation. The effect of continuous transport of slabs on their temperature-distance history along the furnace was simulated by a series of discrete pushes. At each push, one slab is discharged, and the positions of all remaining slabs (together with their nodal temperatures) within the furnace are shifted forward and towards the discharge end. The first slab position at the charge end is then substituted with a new slab at ambient temperature. Operating conditions can also be changed at a specific point in time if necessary, such as production rate. At the end of each time-step, the quadratic flow model (described in Section 2.1) re-calculates the flow pattern inferred by new burner fuel flow rates, which in turn are modulated by the temperature controller at the beginning of each time-step. Figure 5 shows the overall flow chart of the transient furnace model.

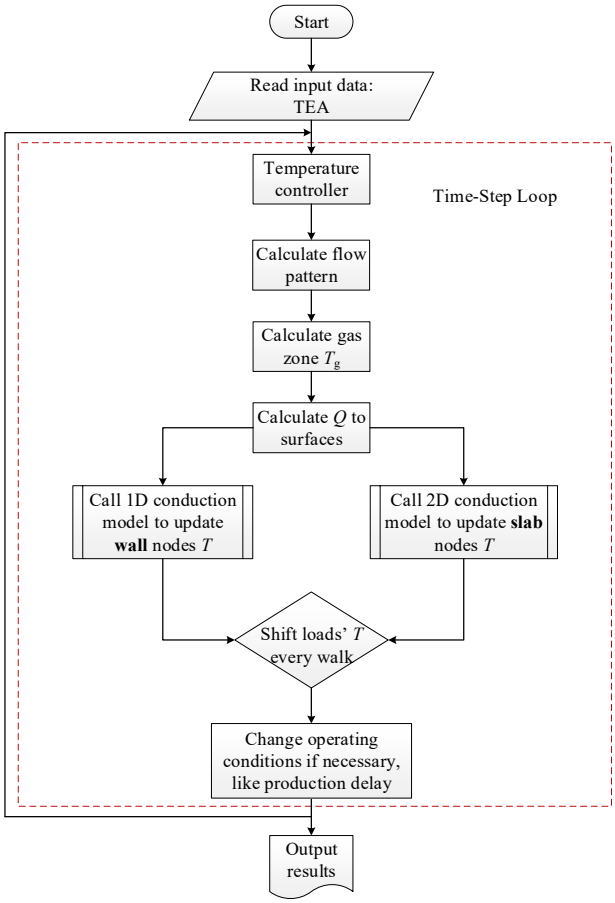

Figure 5. Program flow-chart of the transient furnace model

In this study, the main procedure in solving the above equations requires first to determine all inter-zone mass flow rates within the furnace (which relate to the enthalpy transport term in *Eq. 1* and *Eq. 2*) followed by all directed flux areas from *Eq. 3* through to *Eq. 6*. The authors' previous work [57] on the same furnace had successfully established a quadratic flow model as mentioned in Section 2.1. The same flow model can also be applied here under oxy-fuel combustion conditions so long as a single total mass flow rate (fuel plus oxygen) is specified for each burner. On the other hand, the concentration of radiating gases (i.e. H_2O and CO_2) can be markedly different under air-fuel and oxy-fuel combustion atmosphere, and consequently the total emissivities of the gaseous mixture under oxy-fuel combustion conditions need to be re-determined accordingly.

The standard method used to calculate the total emissivity of participating non-grey gaseous mixture contained in an enclosure is by means of the weighted sum of the emissivities of a number of grey gases (WSGG), represented by *Eq*. 7.

$$\varepsilon_{\mathrm{g}} = \sum_{n=1}^{N} a_{\mathrm{g,n}}(T_{\mathrm{g}})\left[1 - \exp(-k_{\mathrm{g,n}} pL)\right], \qquad (Eq.\ 7)$$

where n = 1 represents the clear ($k_{g,1} = 0$) gas and $n = 2$ to N represent the grey gases; $a_{\mathrm{g,n}}$ is the weighting coefficient; $k_{\mathrm{g,n}}$ is the absorption coefficient, $\mathrm{m^{-1}\ atm^{-1}}$; p is the sum of the partial pressures of radiating gases ($p_{\mathrm{H2O}} + p_{\mathrm{CO2}}$), atm; L is the mean beam length, cm. The following widely used formula (*Eq*. 8) [55] can be applied to calculate the mean beam length L.

$$L = 3.5\frac{V}{A}, \qquad (Eq.\ 8)$$

where V is the volume of the gas and A is its total bounding areas.

It has been shown that the total emissivity of non-grey participating media in furnace enclosure can be derived from Statistical Narrow Band (SNB) model with reasonable accuracy [58]. The constant $25\mathrm{cm}^{-1}$ spectral resolution adopted in the SNB model has been demonstrated to be sufficiently narrow to assume a constant Planck function inside each band for a given temperature in the range of 27 °C to 2227 °C. The SNB model was first used to generate the *ε-pL* data at different temperatures covering the operating conditions in this study, as listed in Table 2. The actual *ε-pL* data at different temperatures T_{gas} are listed in appended Table A.1.

Table 2. Input parameters to the SNB model

	T_{gas}, °C	T_{atm}, °C	p_{CO2}, atm	p_{H2O}, atm	p, atm	L, cm
Air-fuel	2400	27	0.106	0.142	1.0	83.32
Oxy-fuel	2400	27	0.416	0.555	1.0	83.32

A four-term (one clear plus three grey gases) WSGG model was derived using these *ε-pL* data to determine the corresponding grey gas parameters. In this case the weighting coefficients ($a_{g,n}$) were described by a fourth order polynomials in T_g (*Eq*. 9)

$$a_{\mathrm{g,n}}(T_{\mathrm{g}}) = b_{1,\mathrm{n}} + b_{2,\mathrm{n}}T'_{\mathrm{g}} + b_{3,\mathrm{n}}{T'}_{\mathrm{g}}^{2} + b_{4,\mathrm{n}}{T'}_{\mathrm{g}}^{3} + b_{5,\mathrm{n}}{T'}_{\mathrm{g}}^{4} \qquad (Eq.\ 9)$$

where $T'_{\mathrm{g}} = \dfrac{T_{\mathrm{g}} - MU_1}{MU_2}$

is the normalised gas temperature ($MU_1 = 1300$ and $MU_2 = 721.11$) for improved polynomial fit. The polynomial fits for the weighting coefficients are shown in Figure 6, and their corresponding correlation coefficients $b_{1,\mathrm{n}}$, $b_{2,\mathrm{n}}$,…, $b_{5,\mathrm{n}}$ are given in Table 3.

Similarly, acceptable accuracy can be achieved by assuming that $a_{s,n}$ (in *Eq. 5* and *Eq. 6*) is dependent only on the temperature of the emitting surfaces [42]. Therefore,

$$a_{\mathrm{s,n}}(T_{\mathrm{s}}) = b_{1,\mathrm{n}} + b_{2,\mathrm{n}}T'_{\mathrm{s}} + b_{3,\mathrm{n}}{T'}_{\mathrm{s}}^{2} + b_{4,\mathrm{n}}{T'}_{\mathrm{s}}^{3} + b_{5,\mathrm{n}}{T'}_{\mathrm{s}}^{4} \qquad (Eq.\ 10)$$

where, $b_{1,\mathrm{n}}$, $b_{2,\mathrm{n}}$,…, $b_{5,\mathrm{n}}$ are the same coefficients as used in *Eq. 9* and listed in Table 3.

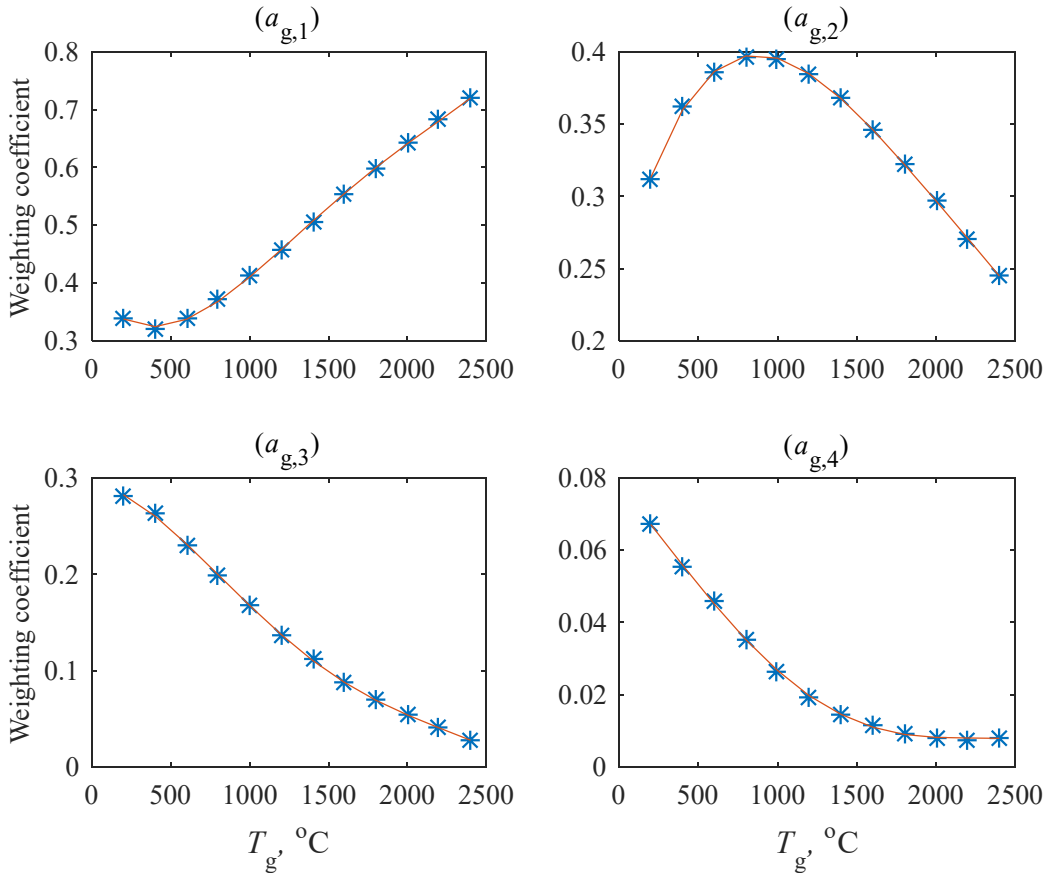

Figure 6. Polynomial fitting of weighting coefficients using the WSGG model

Table 3. Reproduced grey gas parameters used in the mixed grey gas model

	$b_{1,\mathrm{n}}$	$b_{2,\mathrm{n}}$	$b_{3,\mathrm{n}}$	$b_{4,\mathrm{n}}$	$b_{5,\mathrm{n}}$	$k_{\mathrm{g,n}}$, $\mathrm{m^{-1}\ atm^{-1}}$
1	4.83E-01	1.78E-01	-2.08E-03	-2.25E-02	9.36E-03	0.00E+00
2	3.77E-01	-6.22E-02	-3.42E-02	1.72E-02	-3.40E-03	9.10E-01
3	1.23E-01	-9.67E-02	2.50E-02	5.67E-03	-4.92E-03	1.21E+01
4	1.69E-02	-1.88E-02	1.13E-02	-2.86E-04	-1.05E-03	322.21

Figure 7 shows the four-term WSGG model of the total emissivity of combustion products in the range of 200-2400 °C, where the symbols represent data derived from the SNB model and the solid lines represent data calculated from the WSGG model (*Eq*. 5). The standard deviation of the values of total emissivity estimated by the WSGG model under the designed furnace operating conditions (600 to 1350 °C; 0.18 atm·m to 0.78 atm·m) is less than 6%. It can be observed that oxy-fuel combustion conditions result in higher total emissivity for the products of combustion than that of air-fuel cases, due to the higher concentration of CO_2 and H_2O gases.

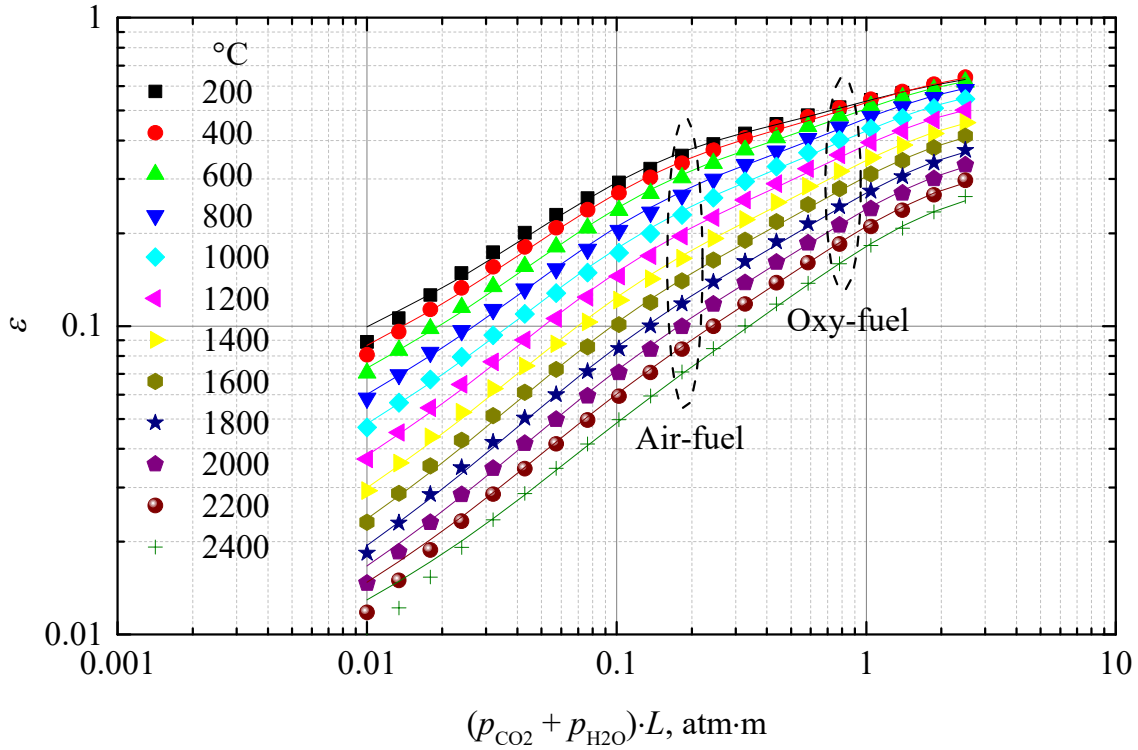

Figure 7. Four-term mixed grey gas fitting to total emissivity of combustion products at different temperatures (symbols: SNB model data; solid line: WSGG model of this study)

5. Results, analysis and discussion

The developed furnace model was first validated using the heating curves collected during the trials. This was followed by illustration (using contour plots or line graphs) of the main heat transfer characteristics, which includes the gas temperature distribution, maximum temperature difference and temperature distribution within the slabs. Finally, energy balance of the furnace was investigated to estimate the energy saving potential from implementing oxy-fuel combustion.

5.1 Validation with the trial data

Figure 8 shows the comparison of the predicted top, centre, and bottom temperature histories of the slab to those of the measured data. In general, the predicted temperature profiles are in good agreement with measured data. However, since a two-dimensional heat conduction model was assumed, the predicted average surface heat flux on the slab is somewhat higher than that experienced at the middle section but lower than that towards both ends where the effect of end-heating from the hot refractory wall is more significant. In addition, oxide formation on the slab surface, which was not

taken into account by the model, also contributed to uncertainty in the material properties as the oxide scales covering the slab surface have a much lower thermal conductivity. The discrepancies between the predicted (i.e. average over the entire length of slab) and actual (i.e. thermocouple point measurements as illustrated in Figure 3) slab temperatures was slightly worst on the top surface given the top-fired nature of the furnace. The overall heating time under oxy-fuel combustion was found to be approximately 13 minutes less than that of air-fuel combustion, which is in close agreement with the actual saving of 14 minutes observed during the experiment. This reduction in the heating time implies an increase in productivity or a decrease in the specific fuel consumption.

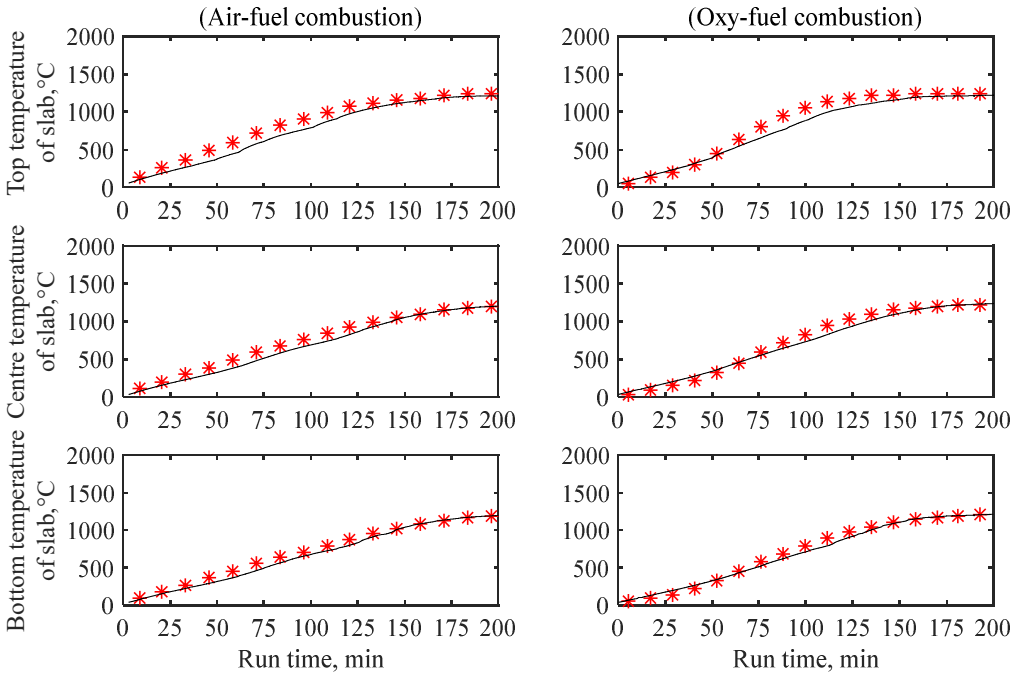

Figure 8. The top (TC1), centre (TC2) and bottom (TC3) temperature histories of the instrumented slab (left column: air-fuel combustion; right column: oxy-fuel combustion; red symbol: prediction; black line: trial data)

5.2 Heat transfer characteristics

Figure 9 shows the steady-state gas temperature contour where it can be clearly observed that the gas temperature in the Dark Zone under the oxy-fuel combustion environment is significantly lower. This can be explained by the fact that to maintain the same heat transfer to the slabs, a smaller firing rate is required compared to the case for air-fuel combustion, and this typically results in a drop in the flue gas temperature. In addition, since the set point temperatures for Control Zones 2 and 3 are kept the same in both combustion environments, their maximum gas temperatures were comparable. The only difference is that for oxy-fuel combustion higher average gas temperatures could be maintained, notably in Control Zone 2. This is believed to be due to the effect of less dilution from nitrogen as would be experienced in air-fuel combustion.

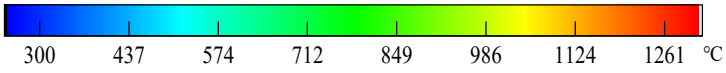

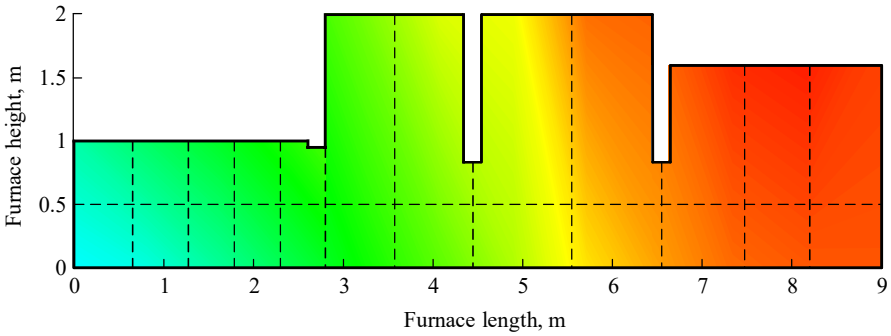

(a) Air-fuel combustion

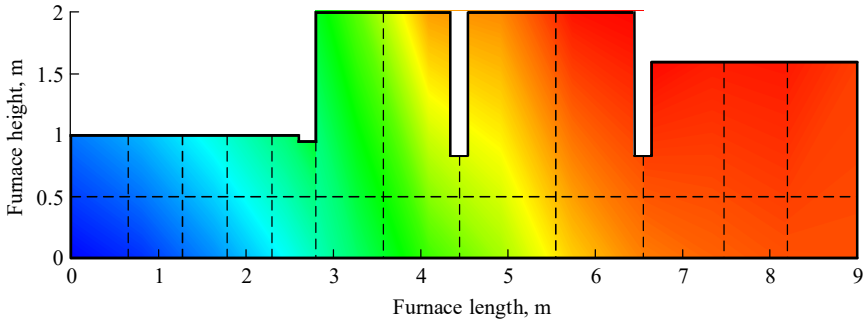

(b) Oxy-fuel combustion

Figure 9. Gas temperature contour when the furnace reached the steady state

The predicted and measured maximum temperature differences within the instrumented slab during reheating process in both combustion environment cases are presented in Figure 10. It is worth mentioning that the measurement points (TC1, TC2, …, TC5) within the instrumented dummy slab are fewer in number than the nodal points of the modelled slab (see Figure 11) and that their locations do not necessarily coincide with one another. For this reason, it was difficult to comment on the discrepancies between the predicted and actual results. However, the observed differences in the trends between the air-fuel and oxy-fuel cases, from both the predictions and actual measurements, were comparable. In particular, both results (model and actual) are in good agreement on higher through-thickness temperature difference initially in the oxy-fuel case, due to its higher heating rate; the difference is almost eliminated in the soak zone. The top-fired nature of this furnace can also be seen clearly from the uneven top-centre and bottom-centre temperature gradient, as evident in Figure 11.

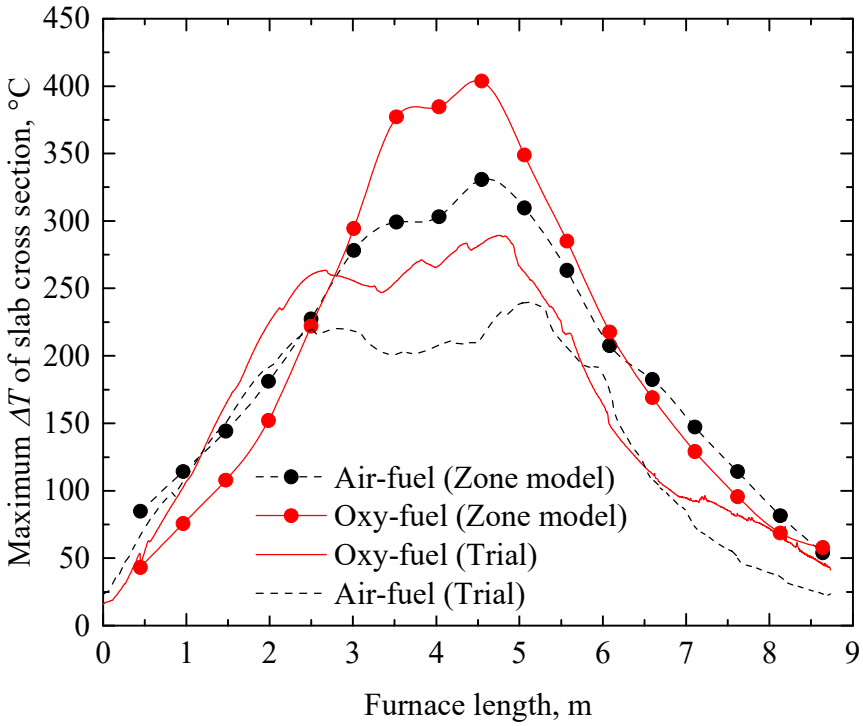

Figure 10. Predicted- and measured maximum temperature difference in the instrumented slab

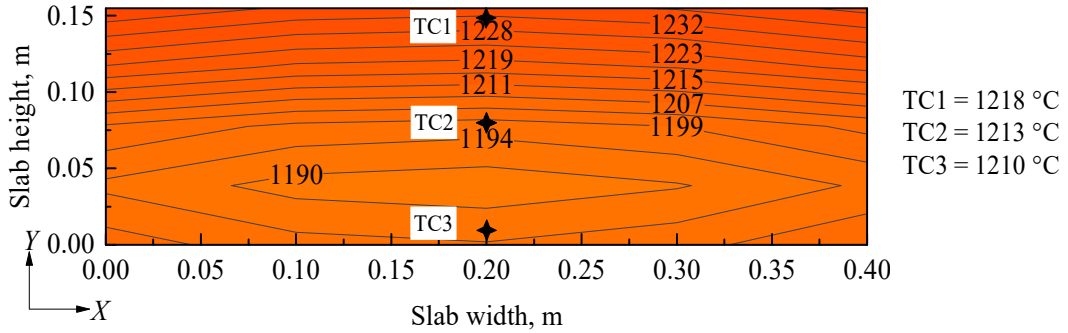

(a) Air-fuel combustion

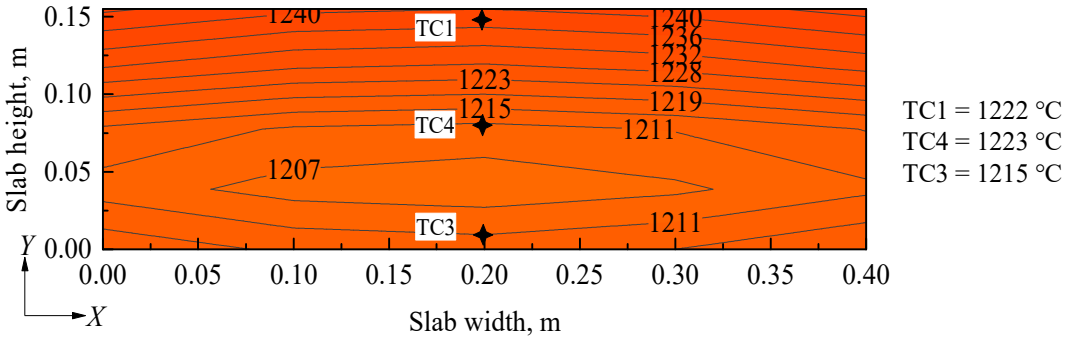

(b) Oxy-fuel combustion

Figure 11. Cross-section temperature contour of the last slab (in same colour scale as Figure 9; ✦ indicates thermocouple locations)

5.3 Furnace energy balance

During simulation of the trial period, the cumulative thermal energy both entering and leaving the furnace were also calculated, as shown in Table 4, and these were compared with the energy balance derived from conventional combustion (air-fuel) [57]. The oxy-fuel case has a significantly smaller exhaust energy loss (Q_e) due mainly to the absence of nitrogen in the combustion along with lower flue gas temperature. As a result, the furnace efficiency is substantially improved by about 20%. The specific fuel consumption has therefore dropped from 1.13 GJ tonne^{-1} to 0.94 GJ tonne^{-1}. This result shows that with oxy-fuel combustion, the specific fuel consumption for reheating steel to the target temperature of around 1250 °C can be improved to below 1.0 GJ tonne^{-1} theoretically, due to the inherent advantages of the technology such as enhanced radiation heat transfer and the absence of heat loss due to nitrogen.

Table 4. Simulation comparison of furnace energy balance by air-fuel combustion and oxy-fuel combustion

		Energy input		Energy output			Performance			
	Units	Q_f	$Q_{o/a}$	Q_s	Q_e	Q_l	E_c	E_f	*SFC*	*Cap.*
Oxy-fuel	MW	1.09	0.02	1.00	0.04	0.09	98.22	91.71	0.94	4.20
	%Q_f	100.00	1.50	91.71	3.28	7.84				
Air-fuel	MW	1.24	0.06	0.94	0.27	0.09	82.74	75.42	1.13	3.95
	%Q_f	100.00	4.42	75.42	21.68	6.86				

Q_f, fuel energy input.
$Q_{o/a}$, preheated oxygen or air energy input
Q_s, energy transferred to steel slabs.
Q_e, energy in exhaust gases as they leave the furnace.
(continued)
Q_l, energy losses to furnace walls.
E_c, combustion efficiency, $1+(Q_{o/a}/Q_f)-(Q_e/Q_f)$ as a percentage.
E_f, furnace efficiency, Q_s/Q_f as a percentage.
SFC, specific fuel consumption, Q_f/tonnes, usually expressed in GJ tonne^{-1}.
Cap., reheating capacity in tonne hr^{-1}.

6. Further remarks on the benefits of oxy-fuel combustion

Since a considerable amount of energy is required for the production of oxygen, this needs to be taken into account in the overall heating cost. On a basis of one tonne of steel produced (Table 5), the amount of additional energy consumption from oxygen production is 0.058 GJ tonne^{-1}, which accounts for about 6% of the furnace specific fuel consumption. Therefore, the total specific energy consumption (0.998 GJ tonne^{-1}, fuel plus oxygen production) is still 12% lower than that of air-fuel combustion case. Further savings would materialise should the cost of carbon capture be taken into consideration. Based on mass balance, with oxy-fuel combustion technology the CO_2 emission per tonne of steel heated is 60.72 kg, that is, the energy consumption for capture is 0.96 MJ kg$^{-1}CO_2$; with air-fuel combustion technology the CO_2 emission per tonne of steel heated is 73.04 kg. However, currently the energy consumption for capture with post-combustion is generally 3.5–4.2 MJ kg$^{-1}CO_2$ [59–61], which means an additional consumption of 0.213-0.255 GJ tonne^{-1} steel is required unless this energy can be recovered somewhere else, such as the recovering sensible heat from continuous casting processes [62]. In contrast, oxy-fuel combustion capture technology is more promising than post-combustion capture technology, which not only has lower carbon capture costs but also enhances heat transfer.

Table 5. Specific energy consumptions, carbon emission and capture cost with different combustion technology

	Unit	Air-fuel	Oxy-fuel	Converter
Specific fuel consumption	GJ tonne^{-1}	1.13	0.94	
				46.40 MJ kg^{-1} (fuel caloric value)
	kg tonne^{-1}	24.35	20.26	
				44.1 kg kmol^{-1} (fuel molar mass)
	kmol tonne^{-1}	0.55	0.46	
			5 (O_2 to fuel stoichiometric ratio); 4% (excess O_2)	
Specific O_2 consumption	kmol tonne^{-1}		2.39	
				32 kg kmol^{-1} (O_2 molar mass)
	kg tonne^{-1}		76.44	
				1.331 kg Nm^{-3} (O_2 density)
	Nm^3 tonne^{-1}		57.43	
				0.28 kWh Nm^{-3} (O_2 production)
	kWh tonne^{-1}		16.08	
				0.0036 (kWh to GJ)
	GJ tonne^{-1}		0.058	
CO_2 emission	kg tonne^{-1}	73.04	60.72	
Energy consumption	MJ kg^{-1} CO_2	3.5–4.2	0.96	

7. Conclusions

This paper first reviewed previous work on reheating furnace modelling, control, and optimisation. A comprehensive mathematical model of the reheating furnace was further developed to simulate oxy-fuel combustion conditions. The developed model was validated using experimental data collected from a pilot-scale walking beam furnace. From both the experimental and simulation results it was found that the specific fuel consumption reduces by about 16% (0.18 GJ tonne^{-1}) and the heating time decreases by about 6% (13 minutes), due to the significant advantages of low exhaust energy loss and enhanced radiation heat transfer in oxy-fuel combustion. From the perspective of carbon capture, oxy-fuel combustion technology can result in reduction of CO_2 emissions by 12.32 kg for heating per tonne of steel heated. Should carbon capture be considered, the energy consumption per kilogram of CO_2 captured can be reduced from 3.5–4.2 MJ kg^{-1} to 0.96 MJ kg^{-1}. These results indicate that oxy-fuel combustion retrofitting to reheating furnaces is a promising option, both from a technical and from an environmental point of view.

Acknowledgements

The authors would like to express their gratitude to the Engineering and Physical Sciences Research Council (EPSRC, EP/P004636/1), UK and the National Natural Science Foundation of China (61573381) for the financial support for this work.

Declarations of interest: none

Nomenclature

Abbreviations

CFD	Computational Fluid Dynamic
CZs	Control Zones
DOC	Dilute Oxygen Combustion
FGR	Flue Gas Recirculation
PID	Proportional–Integral–Derivative
SNB	Statistical Narrow Band
TC	ThermoCouples
WSGG	Weighted Sum of the emissivities of a number of Grey Gases

Symbols

$a_{g,n,}$	weighting coefficient in mixed grey gas model	-
A	total bounding areas	m^2
A_i	area of the i-th surface zone	m^2
b_1, b_2, …, b_5	correlation coefficients	-
Cap.	reheating capacity	tonne hr^{-1}
E_c	combustion efficiency	-
E_f	furnace efficiency	-
$\overline{G_1G_j}, \overline{G_1S_j}, \overline{S_1G_j}, \overline{S_1S_j}$	total exchange areas	m^2
$\overleftarrow{G_1G_j}, \overleftarrow{G_1S_j}, \overleftarrow{S_1G_j}, \overleftarrow{S_1S_j}$	directed flux area	m^2
$k_{g,n}$	grey gas absorption coefficient	$m^{-1}atm^{-1}$
K	radiation attenuation coefficient	-
L	mean beam length	cm
MU1, MU2	centring and scaling parameters	-
p	sum of the partial pressures of radiating gases	atm
$\dot{q}_{conv}$	heat flux to a surface zone by convection	W m^{-2}
$\dot{Q}_a$	heat release from air	W
$\dot{Q}_{conv}$	heat convection	W
Q_e	energy in exhaust gases as they leave the furnace	MW
$\dot{Q}_{enth}$	enthalpy transport term	W
Q_f	fuel energy input	MW
$\dot{Q}_{fuel,net,i}$	heat input of fuel	W
Q_l	energy losses to furnace walls	
$Q_{o/a}$	preheated oxygen or air energy input	MW
Q_s	energy transferred to steel slabs	MW
$\dot{Q}_s$	net heat received by surface zone	W
SFC	specific fuel consumption	MW
T_g	temperature of gas zone	°C
T_s	temperature of surface zone	°C
V	volume of the gas	m^3
V_i	volume of the i-th gas zone	m^3
σ	Stefan-Boltzmann constant (5.6687×10^{-8})	W m^{-2} K^{-4}
ε	emissivity	-

Table A.1 ε-pL data at different temperatures T_{gas}

$p.L$ (atm.m)	L (cm)	T_{gas}. (°C)/ $p.L$ (atm.m)	200	400	600	800	1000	1200	1400	1600	1800	2000	2200	2400
0.0100	1.0299	0.01	0.088767	0.080686	0.070447	0.058431	0.046896	0.037086	0.029230	0.023088	0.018346	0.014668	0.011802	0.009550
0.0134	1.3772	0.01337234	0.106171	0.095797	0.083415	0.069576	0.056414	0.045138	0.035979	0.028699	0.022995	0.018512	0.014980	0.012180
0.0179	1.8416	0.01788194	0.126065	0.113179	0.098229	0.082221	0.067198	0.054305	0.043733	0.035217	0.028456	0.023077	0.018792	0.015362
0.0239	2.4627	0.02391234	0.148483	0.133038	0.115157	0.096615	0.079437	0.064709	0.052568	0.042695	0.034774	0.028406	0.023281	0.019141
0.0320	3.2931	0.03197639	0.173354	0.155510	0.134457	0.113058	0.093405	0.076566	0.062637	0.051236	0.042020	0.034553	0.028494	0.023558
0.0428	4.4037	0.04275992	0.200484	0.180619	0.156333	0.131859	0.109440	0.090187	0.074196	0.061035	0.050338	0.041623	0.034509	0.028676
0.0572	5.8888	0.05718001	0.229569	0.208258	0.180882	0.153272	0.127887	0.105939	0.087588	0.072387	0.059967	0.049803	0.041471	0.034603
0.0765	7.8747	0.07646304	0.260213	0.238179	0.208061	0.177442	0.149026	0.124180	0.103192	0.085656	0.071234	0.059374	0.049611	0.041527
0.1022	10.5303	0.10224897	0.291964	0.270014	0.237677	0.204362	0.173011	0.145177	0.121344	0.101206	0.084498	0.070670	0.059230	0.049703
0.1367	14.0814	0.13673079	0.324354	0.303310	0.269402	0.233854	0.199824	0.169051	0.142265	0.119324	0.100081	0.084020	0.070643	0.059422
0.1828	18.8302	0.18284104	0.356941	0.337583	0.302809	0.265593	0.229265	0.195736	0.166009	0.140162	0.118197	0.099678	0.084125	0.070955
0.2445	25.1804	0.24450124	0.389343	0.372368	0.337428	0.299142	0.260974	0.224981	0.192446	0.163696	0.138914	0.117778	0.099853	0.084505
0.3270	33.6720	0.32695533	0.421265	0.407261	0.372805	0.334021	0.294483	0.256383	0.221266	0.189727	0.162133	0.138306	0.117882	0.100173
0.4372	45.0274	0.43721575	0.452509	0.441952	0.408549	0.369763	0.329286	0.289451	0.252039	0.217908	0.187599	0.161099	0.138129	0.117946
0.5847	60.2121	0.58465971	0.482977	0.476241	0.444360	0.405969	0.364917	0.323696	0.284296	0.247818	0.214967	0.185890	0.160405	0.137714
0.7818	80.5177	0.78182676	0.512672	0.510040	0.480025	0.442330	0.400996	0.358705	0.317623	0.279065	0.243887	0.212386	0.184481	0.159324
1.0455	107.6710	1.04548523	0.541694	0.543357	0.515411	0.478610	0.437240	0.394177	0.351718	0.311364	0.274103	0.240368	0.210178	0.182657
1.3981	143.9813	1.39805826	0.570227	0.576262	0.550428	0.514617	0.473422	0.429888	0.386386	0.344554	0.305492	0.269749	0.237438	0.207705
1.8695	192.5366	1.86953087	0.598517	0.608838	0.584986	0.550150	0.509313	0.465630	0.421467	0.378543	0.338023	0.300546	0.266315	0.234571
2.5	257.4665	2.5	0.626847	0.641120	0.618938	0.584959	0.544628	0.501141	0.456761	0.413213	0.371658	0.332790	0.296894	0.263387

References

[1] International Energy Agency. Energy Technology Perspectives 2012. 2012. doi:10.1787/energy_tech-2012-en.

[2] Chowdhury JI, Hu Y, Haltas I, Balta-Ozkan N, Matthew G, Varga L. Reducing industrial energy demand in the UK: A review of energy efficiency technologies and energy saving potential in selected sectors. Renew Sustain Energy Rev 2018;94:1153–78. doi:10.1016/j.rser.2018.06.040.

[3] Eketorp S. Energy considerations of classical and new iron- and steel-making technology. Energy 1987;12:1153–68. doi:10.1016/0360-5442(87)90070-3.

[4] Broughton JS, Mahfouf M, Linkens DA. A paradigm for the scheduling of a continuous walking beam reheat furnace using a modified genetic algorithm. Mater Manuf Process 2007;22:607–14. doi:10.1080/10426910701323243.

[5] Tang L, Ren H, Yang Y. Reheat furnace scheduling with energy consideration. Int J Prod Res 2015;53:1642–60. doi:10.1080/00207543.2014.919418.

[6] Hu Y, Tan CK, Broughton J, Roach PA, Varga L. Model-based multi-objective optimisation of reheating furnace operations using genetic algorithm. Energy Procedia 2017;142:2143–51. doi:10.1016/j.egypro.2017.12.619.

[7] Gao B, Wang C, Hu Y, Tan CK, Roach PA, Varga L. Function value-based multi-objective optimisation of reheating furnace operations using Hooke-Jeeves algorithm. Energies 2018;11:2324. doi:10.3390/en11092324.

[8] Hu Y, Tan CK, Broughton J, Roach PA. Development of a first-principles hybrid model for large-scale reheating furnaces. Appl Energy 2016;173:555–66. doi:10.1016/j.apenergy.2016.04.011.

[9] Hu Y, Tan CK, Broughton J, Roach PA, Varga L. Nonlinear dynamic simulation and control of large-scale reheating furnace operations using a zone method based model. Appl Therm Eng 2018;135:41–53. doi:10.1016/j.applthermaleng.2018.02.022.

[10] Pili R, Romagnoli A, Spliethoff H, Wieland C. Techno-Economic Analysis of Waste Heat Recovery with ORC from Fluctuating Industrial Sources. Energy Procedia 2017;129:503–10. doi:10.1016/j.egypro.2017.09.170.

[11] Jiménez-Arreola M, Pili R, Dal Magro F, Wieland C, Rajoo S, Romagnoli A. Thermal power fluctuations in waste heat to power systems: An overview on the challenges and current solutions. Appl Therm Eng 2018;134:576–84. doi:10.1016/j.applthermaleng.2018.02.033.

[12] Chen D, Lu B, Dai FQ, Chen G, Zhang X. Bottleneck of slab thermal efficiency in reheating furnace based on energy apportionment model. Energy 2018;150:1058–69. doi:10.1016/j.energy.2018.02.149.

[13] Piotr J, Kiedrzyńska A, Badyda K. CFD analysis of natural gas substitution with syngas in the industrial furnaces. Energy 2019. doi:10.1016/j.energy.2019.04.179.

[14] Kilinç E, Kaya D, Kiliç FÇ, Eyidoğan M, Özkaymak M, Taylan O, et al. An energy efficiency analysis of an industrial reheating furnace and an implementation of efficiency enhancements methods. Energy Explor Exploit 2014;32:989–1003. doi:10.1260/0144-5987.32.6.989.

[15] Oliveira FAD, Carvalho JA, Sobrinho PM, de Castro A. Analysis of oxy-fuel combustion as an alternative to combustion with air in metal reheating furnaces. Energy 2014;78:290–7. doi:10.1016/j.energy.2014.10.010.

[16] Conti J, Holtberg P, Diefenderfer J, LaRose A, Turnure JT, Westfall L. International Energy

Outlook 2016 With Projections to 2040. vol. 0484. 2016. doi:10.2172/1296780.
[17] Wagner D. Science and Civilisation in China: Vol. 5, Part 11: Ferrous Metallurgy. Cambridge University Press; 2008.
[18] Chater WJB. Oxygen processes in the steel industry. Chem Eng Sci 1954;3:IN5-117. doi:10.1016/S0009-2509(54)80010-8.
[19] Stokes RG. Building Upon Air: A History of the International Industrial Gases Industry from the 19th to the 21st Centuries. Cambridge: Cambridge University Press; 2015.
[20] Newell WC. Application of oxygen to steel-making. Nature 1948:439–40. doi:10.1038/162680a0.
[21] Abraham BM, Asbury JG, Lynch EP, Teotia APS. Coal–oxygen process provides CO2 for enhanced recovery. Oil Gas J 1982;80:68–70, 75.
[22] Hu Y, Yan J. Characterization of flue gas in oxy-coal combustion processes for CO2 capture. Appl Energy 2012;90:113–21. doi:10.1016/j.apenergy.2011.03.005.
[23] Castle WF. Air sepration and liquefaction: Recent developments and prospects for the beginning of the new millennium. Int J Refrig 2002;25:158–72. doi:10.1016/S0140-7007(01)00003-2.
[24] US DoE. Dilute oxygen combustion: Phase I report, by Praxair, Inc. and Tarrytown, NY. 1997.
[25] US DoE. Dilute oxygen combustion: Phase III report, by Praxair, Inc. and Tarrytown, NY. 2000.
[26] US DoE. Dilute oxygen combustion: Phase IV report, by Praxair, Inc. and Tarrytown, NY. 2003.
[27] Nicholson R. Recuperative and regenerative techniques at high temperature. J Heat Recover Syst 1983;3:385–404. doi:10.1016/0198-7593(83)90053-X.
[28] US DoE. Dilute oxygen combustion: Phase II report, by Praxair, Inc. and Tarrytown, NY. 2005.
[29] Weinberg FJ. Combustion temperatures: The future? Nature 1971;233:239–41. doi:10.1038/229560a0.
[30] Blasiak W, Yang WH, Narayanan K, von Schéele J. Flameless oxyfuel combustion for fuel consumption and nitrogen oxides emissions reductions and productivity increase. J Energy Inst 2007;80:3–11. doi:10.1179/174602207X174379.
[31] Mortberg M, Tsiava R, Niska J, Rensgard A, Gitzinger J-P, Giese R. Oxy-combustion-a viable solution for reduced emissions and minimized energy consumption. AFRC Int. Symp., Houston, Texas: 2006.
[32] Cavaliere A, De Joannon M. Mild combustion. vol. 30. 2004. doi:10.1016/j.pecs.2004.02.003.
[33] Schéele J Von. Oxyfuel combustion in the steel industry: energy efficiency and decrease of CO2 emissions. Energy Effic., 2010, p. 83–103. doi:10.5772/9830.
[34] Cates L, Browning R. Advnced oxy-fuel burners and controls improve fuel savings and uniform heating. Int J Forg Bus Technol 2011;January:8–11. doi:10.1002/mop.4650021105.
[35] Gangoli S, Buragino G, He X, Arslan E, Verderame P, Hendershot R, et al. Importance of Control Strategy for Oxy-Fuel Burners in a Steel Reheat Furnace. AISTech 2013—Pittsburgh, Pennsylvania, USA—6 May 2013, 2013, p. 1869–73.
[36] Landfahrer M, Schluckner C, Prieler R, Gerhardter H, Zmek T, Klarner J, et al. Numerical and experimental investigation of scale formation on steel tubes in a real-size reheating furnace. Int J Heat Mass Transf 2019;129:460–7. doi:10.1016/j.ijheatmasstransfer.2018.09.110.

[37] Prieler R, Mayr B, Demuth M, Holleis B, Hochenauer C. Numerical analysis of the transient heating of steel billets and the combustion process under air-fired and oxygen enriched conditions. Appl Therm Eng 2016;103:252–63. doi:10.1016/j.applthermaleng.2016.04.091.
[38] Han SH, Lee YS, Cho JR, Lee KH. Efficiency analysis of air-fuel and oxy-fuel combustion in a reheating furnace. Int J Heat Mass Transf 2018;121:1364–70. doi:10.1016/j.ijheatmasstransfer.2017.12.110.
[39] Khalil EE, Spalding DB, Whitelaw JH. The calculation of local flow properties in two-dimensional furnaces. Int J Heat Mass Transf 1975;18:775–91.
[40] Pai BR, Michelfelder S, Spalding DB. Prediction of furnace heat transfer with a three-dimensional mathematical model. Int J Heat Mass Transf 1978;21:571–80.
[41] Hottel HC, Sarofim AF. Radiative transfer. New York: McGraw-Hill; 1967.
[42] Rhine JM, Tucker RJ. Modelling of gas-fired furnaces and boilers. New York: McGraw-Hill; 1991.
[43] Ferreira SLC, Bruns RE, Ferreira HS, Matos GD, David JM, Brandao GC, et al. Box-Behnken design: An alternative for the optimization of analytical methods. Anal Chim Acta 2007;597:179–86. doi:10.1016/j.aca.2007.07.011.
[44] Path tracing. Wikipedia n.d. https://en.wikipedia.org/wiki/Path_tracing (accessed January 9, 2019).
[45] van Leersum J. A method for determining a consistent set of radiation view factors from a set generated by a nonexact method. Int J Heat Fluid Flow 1989;10:83–5.
[46] Lawson DA, Ziesler CD. An accurate program for radiation modelling in the desigh of high-tempersature furnaces. IMA J Manag Math 1996;7:109–16. doi:10.1093/imaman/7.2.109.
[47] Matthew AD, Tan CK, Roach PA, Ward J, Broughton J, Heeley A. Calculation of the radiative heat-exchange areas in a large-scale furnace with the use of the monte carlo method. J Eng Phys Thermophys 2014;87:732–42. doi:10.1007/s10891-014-1067-4.
[48] Howell JR. The Monte Carlo Method in Radiative Heat Transfer. J Heat Transfer 1998;120:547. doi:10.1115/1.2824310.
[49] Hu Y, Wang J, Tan CK, Sun C, Liu H. Coupling detailed radiation model with process simulation in Aspen Plus: A case study on fluidized bed combustor. Appl Energy 2018;227:168–79. doi:10.1016/j.apenergy.2017.08.030.
[50] Galperin EA. Deterministic regression models for prediction and control. Math Model 1985;6:157–71. doi:10.1016/0270-0255(85)90006-5.
[51] Kim Y Il, Moon KC, Kang BS, Han C, Chang KS. Application of neural network to the supervisory control of a reheating furnace in the steel industry. Control Eng Pract 1998;6:1009–14. doi:10.1016/S0967-0661(98)00098-7.
[52] Laurinen P, Röning J. An adaptive neural network model for predicting the post roughing mill temperature of steel slabs in the reheating furnace. J Mater Process Technol 2005;168:423–30. doi:10.1016/j.jmatprotec.2004.12.002.
[53] Liao Y, Wu M, She J-H. Modeling of reheating-furnace dynamics using neural network based on improved sequential-learning algorithm. 2006 IEEE Int. Conf. Control Appl., Munich, Germany, 4-6 October: 2006, p. 3175–81. doi:10.1109/CACSD-CCA-ISIC.2006.4777146.
[54] Yokogawa digital Yewflo vortex flow meters n.d.
[55] Modest MF. Radiative heat transfer. 3rd ed. London: Elsevier Inc.; 2013.
[56] Hildebrand F. Introduction to numerical analysis. Dover Publications; 1987.

[57] Hu Y, Niska J, Broughton J, McGee E, Tan CK, Matthew A, et al. Zone modelling coupled with dynamic flow pattern for the prediction of transient performance of metal reheating. AISTech2014, Indianapolis, USA, 5-8 May: 2014.

[58] Soufiani A, Taine J. High temperature gas radiative property parameters of statistical narrow-band model for H2O, CO2 and CO, and correlated-K model for H2O and CO2. Int J Heat Mass Transf 1997;40:987–91. doi:10.1016/0017-9310(96)00129-9.

[59] Arasto A, Tsupari E, Kärki J, Pisilä E, Sorsamäki L. Post-combustion capture of CO2 at an integrated steel mill - Part I: Technical concept analysis. Int J Greenh Gas Control 2013;16:271–7. doi:10.1016/j.ijggc.2012.08.018.

[60] Sanpasertparnich T, Idem R, Bolea I, deMontigny D, Tontiwachwuthikul P. Integration of post-combustion capture and storage into a pulverized coal-fired power plant. Int J Greenh Gas Control 2010;4:499–510. doi:10.1016/j.ijggc.2009.12.005.

[61] Li K, Leigh W, Feron P, Yu H, Tade M. Systematic study of aqueous monoethanolamine (MEA)-based CO2 capture process: Techno-economic assessment of the MEA process and its improvements. Appl Energy 2016;165:648–59. doi:10.1016/j.apenergy.2015.12.109.

[62] Zhang F, Zhou Y, Sun W, Hou S, Yu L. CO2 capture from reheating furnace based on the sensible heat of continuous casting slabs. Int J Energy Res 2018;42:2273–83. doi:10.1002/er.4020.

https://dspace.org/

Modelling and simulation of steel reheating processes under oxy-fuel combustion conditions – Technical and environmental perspectives

Hu, Yukun; Tan, C. K.; Niska, John; Chowdhury, Jahedul; Balta-Ozkan, Nazmiye ...

2019-07-11
Elsevier
https://doi.org/10.1016/j.energy.2019.07.054
Hu Y, Tan CK, Niska J, et al., (2019) Modelling and simulation of steel reheating processes under oxy-fuel combustion conditions – Technical and environmental perspectives. Energy, Volume 185, October 2019, pp. 730-743

Downloaded from a DSpace repository. https://dspace.org/